國立交通大學
National Chiao Tung University

出國報告（出國類別：出國短期研究）

Combination of Morphological, Interface and Optical Engineering to Achieve Highly-Efficient Polymer Tandem Solar Cells(2)

結合形態工程、界面工程及光學工程達到高效能串疊型高分子太陽能電池(2)

服務機關：應用化學系
姓名職稱：張志宇 博士後研究

前往國家：美國 西雅圖 華盛頓大學材料所
出國期間：**2013/01/01~2013/05/15**
報告日期：**2013/07/09**

摘要

太陽能源技術已被認為是最適合發展之替代能源技術之一，而高分子太陽能電池因其潛在優點如成本低廉、製程簡便、易於大面積化、具撓曲性等，是未來太陽能技術發展之趨勢。欲成為實用替代能源，高分子太陽能電池必須具備足夠光轉化效率，而其中的關鍵因素為調控元件之界面及光學特性。本次短期研究前往美國西雅圖華盛頓大學材料系 Dr. Alex K-Y. Jen 實驗室進行為期約八個月的學術交流，研究目標為結合形態工程、界面工程及光學工程實現高效能串疊型高分子太陽能電池。Dr. Alex K-Y. Jen 的研究團隊在串疊型高分子太陽能電池及半透明高分子太陽能電池元件是世界知名的先驅，研究成果斐然。藉由此次實質的學術交流與合作機制，不僅可提升研究水平達到雙贏局面，也可以開拓跨領域、跨文化的國際視野。

本次短期出國之研究工作，將著重於實現高效能串疊型太陽能電池，內容包括: (1)開發有效之中間連接層以實現高效能串疊型太陽能電池; (2)藉由改變碳球衍生物實現高效率半透明串疊型太陽能電池。經由最佳化製程條件(包括:改變薄膜厚度及成份改質)，研究結果已成功開發可適用於串疊型太陽能電池的中間連接層。結合之前開發出的高效能低能隙高分子，我們成功實現高效能串疊型太陽能電池，元件效率達 8.2%。此外，此次研修也成功開發高效率半透明串疊型太陽能電池，元件之光學穿透度為 39.9%，元件效率為 6.7%，為目前半透明太陽能電池的最高紀錄值。除此之外，所開發的半透明太陽能電池具備高度演色性指標(97.2%)，未來應用於太陽能發電窗戶極具潛力。

目次

本文

一、 目的

隨著非再生能源的漸漸枯竭，以及使用非再生能源所產生環境破壞問題的日趨嚴重，再生能源的開發已成為人類共同的當務之急，世界各國極力發展的各項替代能源包括有太陽能、風能、氫能、地熱能等。我國屬海島型國家，天然資源本已匱乏，目前能源需求有 95% 以上仰賴國外進口，因此在非再生能源緊縮之情況下，所受衝擊將遠大於資源豐饒之工業大國，也因此發展有效的替代能源，將是我國永續生存的唯一選擇。在潛在的替代能源選擇中，尤以太陽能適合我國發展，因臺灣地處亞熱帶地區，日照充沛，太陽能之供給不虞匱乏。就市場經濟面來看，近年來世界太陽能市場銷售總額年成長率皆達 30%以上。目前市面上所生產的太陽電池以無機矽半導體為主，III-V 族、 II-VI 族等材料為輔。此類矽基太陽電池雖已商業化，但其價格在美金＄5/瓦上下，遠不符經濟效益。根據能源工業界估計，太陽電池若欲取代現有供電機制，其價格必須在美金＄1/瓦以下。無機半導體太陽電池之製程已漸趨固定，成本已難再降低。因此找尋一低成本、製程簡易的材料是目前太陽電池的發展關鍵。

高分子太陽能電池具備成本低廉、製程簡易、輕薄、可大面積製備、可撓曲及應用性廣(如:半透明太陽能電池)等優點，近來廣被各界重視並投入研究。然而，高分子太陽能電池距離實際商業化仍然有許多技術上的難題亟待克服，其中一關鍵因素為元件之光電轉換效率仍有待改善。提升元件光電轉換效率的方法主要有下列三項: (1)將兩個不同光譜響應的高分子太陽能電池結合形成串疊型太陽能電池，增加太陽光譜中的波長利用率；(2)導入分子修飾層於有機半導體及電極之界面，改善界面缺陷以及功函數不匹配之問題，進而提升載子之收集；(3)藉由光學工程(如:調控材料之光學特性)使入射光侷限在元件內部中，增加光路長度(optical path length)，提升光子吸收機率。目前串疊型太陽能電池之光電轉換效率達 10.7%，為現有高分子太陽能電池之光電轉換效率最高記錄。藉由導入界面

修飾層及調控材料之光學特性於串疊型太陽能電池可望能大幅提升光電轉換效率，但目前卻只有極少的文獻有相關之報導。

本校理學院「前瞻跨領域基礎科學中心」，為教育部邁向頂尖大學計畫中正式核准之頂尖中心，發展下一世代有機太陽能電池為該中心主要目標之一，而美國西雅圖華盛頓大學 Prof. Alex Jen 實驗室，是世界在此領域研究成果領先之團隊，其主要是在串疊型高分子太陽能電池及半透明型高分子太陽能電池有獨特之技術，本次出國短期研究之目的主要是學習 Prof. Alex Jen 團隊在這兩方面之製程技術，將此兩種技術帶回臺灣，可以促進彼此雙方之交流合作，另一方面可以提升「前瞻跨領域基礎科學中心」在下一世代太陽能電池之研究水準。

二、 過程

本人至美國西雅圖華盛頓大學材料系進行交流，在出發前的期間，便與美國西雅圖華盛頓大學材料系的 Alex K-Y. Jen 教授有多次的電子信件連絡，Alex K-Y. Jen 教授也寄給我一些與本交流計畫想關的文獻來進來閱讀。

搭上長榮航空的班機前往美國，在經過十多個小時的飛行之後，便到達了美國華盛頓州的西雅圖機場，當天天氣不是很好，有點下雨，Alex K-Y. Jen 教授有請他的博士後研究員來幫我接機，並幫我安排暫時居住的地方。並且帶我在當地的超市進行簡單的採買。

在到達西雅圖的隔天，就先參觀了美國西雅圖華盛頓大學的校園，這個校園非常的漂亮，雖然之前已經在網路上看過，但是親眼看到不同系所的建築物都是各有特色。最後看到了我主要訪問的材料系，就馬上與 Alex K-Y Jen 教授進行面談，Alex K-Y. Jen 教授主要的的研究方向是串疊型高分子太陽能電池及半透明

高分子太陽能電池元件，經過了約兩個小時的談話後，Alex K-Y Jen 教授與我擬定了未來的研究方向。

根據我們那一天討論的結果，主要的研究方向分成兩個部份，包括: (1)開發有效之中間連接層以實現高效能串疊型太陽能電池; (2)藉由改變碳球衍生物實現高效率半透明串疊型太陽能電池。為實現高效能串疊型太陽能電池，其中的兩個關鍵因素為高效能低能隙高分子及有效之中間連接層。在之前的研究中，我們藉由結合形態工程、界面工程以及光學工程，已開發高效能之低能隙高分子太陽能電池，元件效率達 6.6%，為目前該系列材料(cyclopenta[2,1-b;3,4-b′] dithiophene,CPDT)之最高紀錄值。更進一步地，將單層反式高分子太陽能電池堆疊成高效能串疊式高分子太陽能電池，此串疊式高分子太陽能電池技術為目前大部份實驗室所缺乏之製程技術，該製程為目前有機太陽能電池的發展主流。

訂定這兩個主要的研究方向之後，我便參觀了 Alex K-Y Jen 教授的實驗室設備。在之後的幾個星期，主要是跟實驗室裡面的幾個博士後研究員學習太陽能電池的相關製程。我平常所用的詳細製程技術如下所描述：單層反式高分子太陽能電池製程 ： 具有 ITO (indium tin oxide) 的透明玻璃基板(電阻值小於 15 歐姆) ，浸至於清潔劑，去離子水，丙酮和異丙醇各 15 分鐘，接著放在紫外線-臭氧清洗機裡面半小時以達到表面清潔的效果。氧化鋅先驅物溶液由 zinc acetylacetonate hydrate 溶解在乙醇 (20 mg/ml) ，接著用旋轉塗佈的方式附著在 ITO 上，在大氣下進行烤片 130 度 5 分鐘，其厚度約為 40 奈米，做為電子傳輸層。在電子傳輸層上旋轉塗布上富勒烯衍生層作為電洞阻擋層，在將主動層材料 poly[2,6-(4,4- bis(2-ethylhexyl)-4H-cyclopenta dithiophene)-alt-4,7- (5-fluoro-2,1,3-benzothia-diazole)] (PCPDFBT) 與 PC71BM 以 1:2.5 的混摻比例 (28mg/ml)或 Poly(3-hexylthiophene-2, 5-diyl)(P3HT) 與 ICBA 以 1:1 混摻 (34mg/ml)溶解於鄰二氯苯，接著旋轉徒佈上所需的主動層厚度，poly(3,4-ethylenedioxythiophene):poly (styrenesulfonate) (PEDOT:PSS)添加少量界

面活性劑 (Zonyl FSO fluorosurfactant) 旋轉塗佈在主動層上，厚度 30 nm ，在高真空下(小於 10-6 torr 以下)，進行蒸鍍上銀做為接觸電極 (200 nm) ，或半透明電極 (10 nm) 。

串疊型高分子太陽能電池製程 : 其製程方面可分成底部電池與上層電池兩部份。清洗試片步驟與單層反式高分子太陽能電池相同。氧化鋅先驅物溶液由 zinc acetylacetonate hydrate 溶解在乙醇 (20 mg/ml) ，接著用旋轉塗佈的方式附著在 ITO 上，在大氣下進行烤片 130 度 5 分鐘，其厚度約為 40 奈米，做為電子傳輸層。在電子傳輸層上旋轉塗布上富勒烯衍生層作為電洞阻擋層，在將主動層材料 P3HT 與 ICBA 以 1:1 混摻 (34mg/ml) 溶解於鄰二氯苯，接著旋轉徒佈上所需的主動層厚度，進行長時間溶劑淬火，poly(3,4-ethylenedioxythiophene):poly(styrenesulfonate)(PEDOT:PSS)添加少量界面活性劑(Zonyl FSO fluorosurfactant) 旋轉塗佈在主動層上，厚度 30 nm ，旋轉塗佈上 PH1000，厚度約為 30 nm，用甲醇清洗旋轉塗佈好的 PH1000 使其導電性增加，接著進行上層電池的疊加，氧化鋅與富勒烯電洞阻擋層的塗佈方式與下層電池一樣，上層電池中主動層材料使用 PCPDFBT 與 PC71BM 以 1:2.5 的混摻比例 (28 mg/ml) 旋轉塗佈上所需厚度，旋轉塗佈上改質 PEDOT:PSS ，在高真空下(小於 10-6 torr 以下) ，進行蒸鍍上銀做為接觸電。

在熟悉了相關的太陽能元件製程之後，在之後的幾個月中，主要是在開發一些有效的中間連接層材料，其結構為:改質 poly(3,4- ethylenedioxythiophene): poly(styrenesulfonate)(PEDOT:PSS)高導電度 PEDOT:PSS/氧化鋅。此中間連接層具備足夠的溶劑阻抗性(Figure 1)、高度光學穿透性(Figure 2)以及平坦的表面形態(Figure 3)。串疊型元件結構如 Figure 4a 所示，其光電轉換效率達 8.2% (Table 1 及 Figure 4b) ，為目前有機高分子太陽能電池的最高效率值。

此外，在最後的幾個月期間，主要在開發高效率半透明串疊型太陽能電池(元

件結構如 Figure 5)，元件之平均光學穿透度(average visible transmittance, AVT)為 39.9%(Figure 5)，元件效率為 6.7%(Table 2)，為目前半透明太陽能電池的最高紀錄值。除此之外，此新開發的半透明太陽能電池具備高度演色性指標(97.2%，Figure 6)，未來應用於太陽能發電窗戶極具潛力。

在美國西雅圖華盛頓大學材料系交流期間，本人順利的完成了與 Alex K-Y Jen 教授一開始討論的研究方向，也參觀了華盛頓大學材料系與化學系等系所。另外，美國西雅圖華盛頓大學很有名的是其電腦的相關科系，本人也參觀了裡面世界級的電腦設備。之後於 102 年 5 月 15 日，本人向 Alex K-Y Jen 教授實驗室同仁告別，經過十多個小時的航程後，抵達臺灣桃園機場。

在此次的短期交流將有助於開發新穎性之高分子太陽能電池(包括:半透明電池及串疊型電池)及高效能之低能隙材料，不僅可以提升雙方的研究水平，亦可以開拓跨領域、跨文化的國際視野。在研究成果產出部份，目前已有兩篇 SCI 論文被國際知名期刊接受(包括 Polymer Chemistry 及 Advanced Functional Materials)，後續相關的研究成果亦在整理中，預期總共將產出四篇的 SCI 論文。

Table 1. Summary of the photovoltaic device parameters for the sub-cells and tandem cell.

Device	V_{oc} [Volt]	J_{sc} [mA cm^{-2}]	FF [%]	PCE [%]
Front cell	0.83	11.59	68.05	6.5
Rear cell	0.74	14.24	61.68	6.6
Tandem cell	1.57	7.83	66.46	8.2

Table 2. Summary of the photovoltaic device parameters for the tandem cell and semitransparent tandem cell

Ag thickness [nm]	V_{oc}	J_{sc}	FF	PCE	AVT
200	1.71	6.91	65.70	7.8	<0.1
10	1.70	5.81	67.40	6.7	39.9

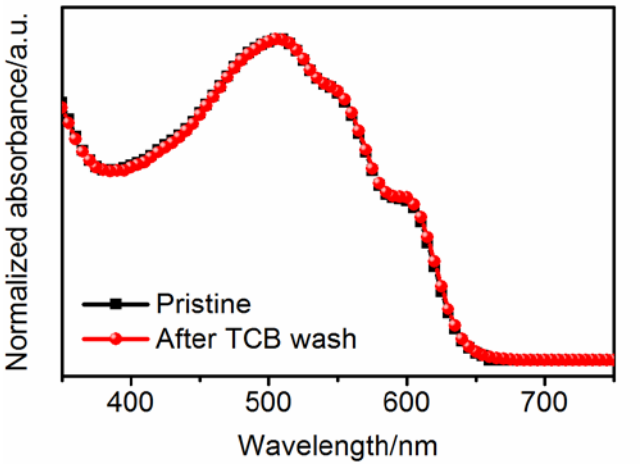

Figure 1. UV-Vis absorption spectra of P3HT:ICBA films before and after being washed with TCB.

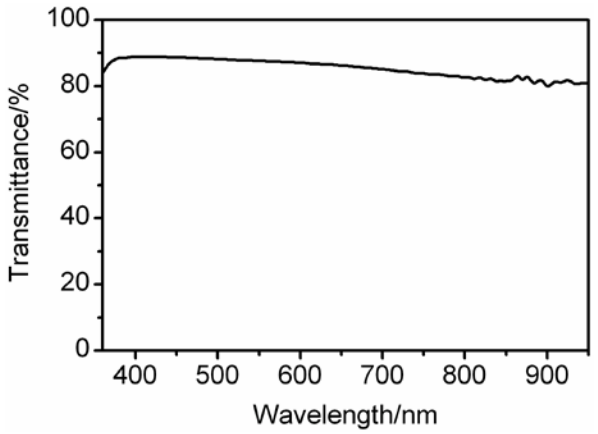

Figure 2. Optical transmittance of ICL used in this study.

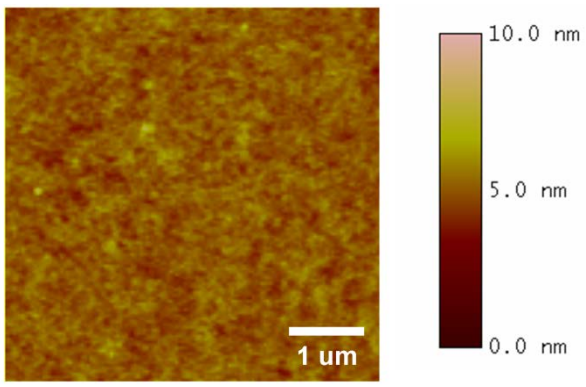

Figure 3. AFM topography images of ICL used in this study (rms roughness = 0.88 nm). The scan size was 5 μm × 5 μm.

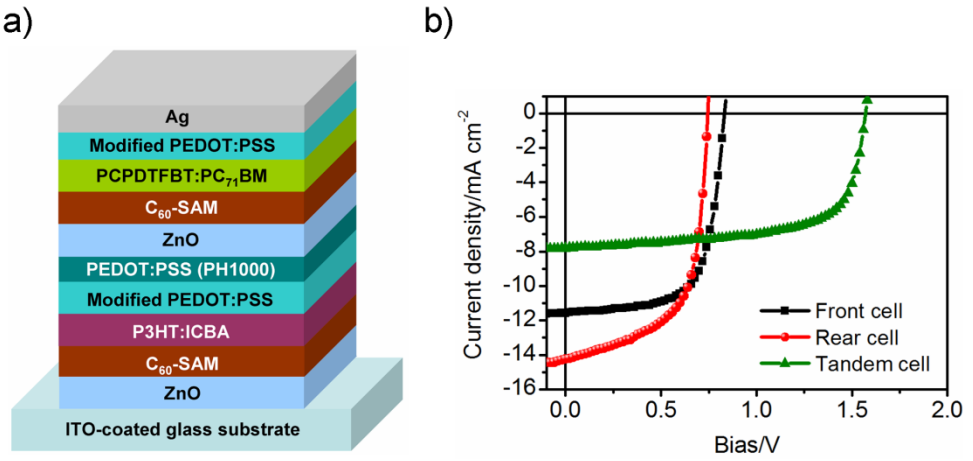

Figure 4. (a) Schematic representation of the device architecture used in this study. (b) *J-V* characteristics of the tandem cell.

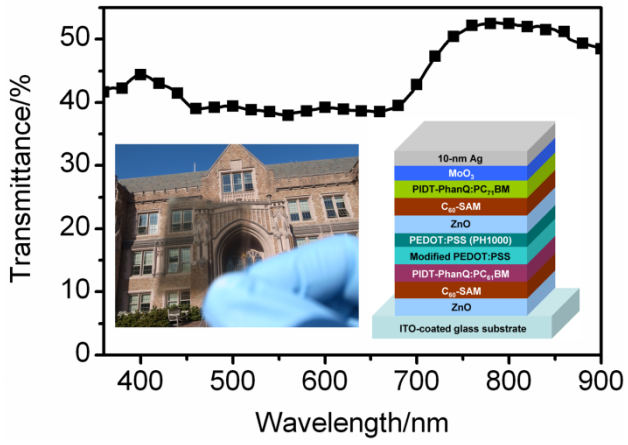

Figure 5. Optical transmittance of the as-fabricated semitransparent tandem cell. The inset shows a photograph of semitransparent tandem cell and its device structure.

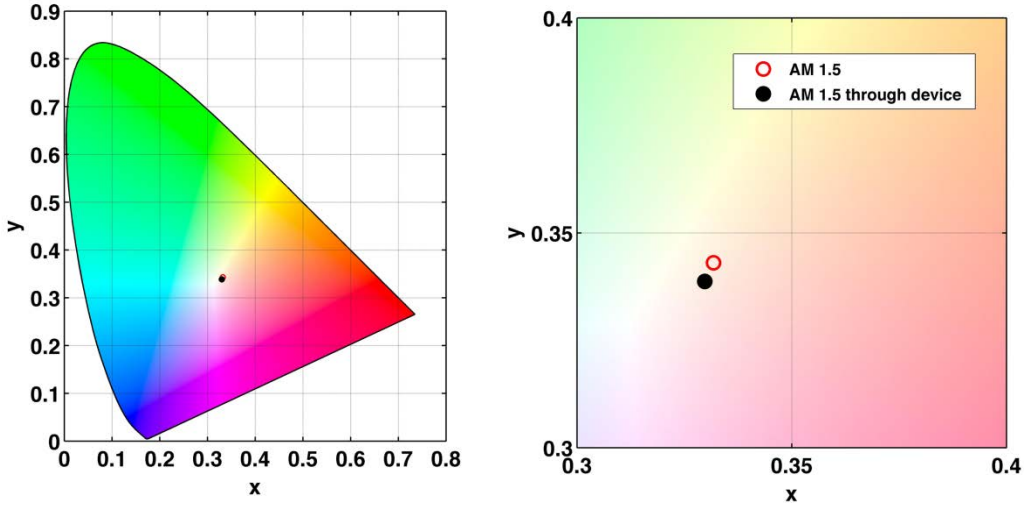

Figure 6. Color rendering index of semitransparent tandem cell demonstrated in this study.

三、心得及建議

個人非常感謝學校有此機會讓本人至美國華盛頓大學材料系交流，透過此次出國進修，雙方已經建立好交流的管道。本人這次在華盛頓大學做有機太陽能元件之研究，與華盛頓大學任廣禹教授團隊共同研究，可以清楚瞭解這個領域是非常競爭的，任廣禹教授團隊下的博士後及博士生都非常認真，其工作精神令人敬佩，從他們身上可以看到他們對於研究工作之熱忱，這是本人所欠缺的。

此外，本人對於此次出國研究有幾點建議:

1. 多派博士班學生出國研究並學習不同實驗室的研究方法與學習態度，可將國外優秀的學術風氣帶回國內以培養更多更優秀的臺灣人才。

2. 除了有優秀的實驗態度和研究方法，也需要良好的實驗儀器來輔佐實驗的進行，這次在 Dr. Alex K-Y Jen 實驗室進行學術交流與研究，了解到國外大學的一流實驗室，貴重儀器與一般研究設備，皆是在臺灣各大學中一整個系的規模。

3. 定期邀請國外優秀學者來國內演講，可以促進彼此間的學術交流，衝擊出更多的跨國學術研究，讓臺灣學者登上國際的舞臺，同時，國外學者也了解到臺灣學術的實力。

4. 此次所學習到串疊型太陽能電池需要用到一些特殊的設備，已建議許千樹教授團隊採用，目前正在找國內廠商設計製造此設備。

四、附錄

以下為出國期間所完成的兩篇論文：

ADFM201301557.xml Generated by PXE using XMLPublish[SM] July 3, 2013 10:33 APT: WF JID: ADFM

ADFM201301557

www.afm-journal.de

A Versatile Fluoro-Containing Low-Bandgap Polymer for Efficient Semitransparent and Tandem Polymer Solar Cells

By Chih-Yu Chang, Lijian Zuo, Hin-Lap Yip, Yongxi Li, Chang-Zhi Li, Chain-Shu Hsu,* Yen-Ju Cheng, Hongzheng Chen,* and Alex K.-Y. Jen*

Keywords: low bandgap polymers, polymer solar cells, tandem solar cells, semitransparent solar cells, organic electronics

The versatility of a fluoro-containing low band-gap polymer, poly[2,6-(4,4-bis(2-ethylhexyl)-4H-cyclopenta[2,1-b;3,4-b']dithiophene)-alt-4,7-(5-fluoro-2,1,3-benzothia-diazole)] (PCPDTFBT) in organic photovoltaics (OPVs) applications is demonstrated. High boiling point 1,3,5-trichlorobenzene (TCB) is used as a solvent to manipulate PCPDTFBT:[6,6]-phenyl-C_{71}-butyric acid methyl ester ($PC_{71}BM$) active layer morphology to obtain high-performance single-junction devices. It promotes the crystallization of PCPDTFBT polymer, thus improving the charge-transport properties of the active layer. By combining the morphological manipulation with interfacial optimization and device engineering, the single-junction device exhibits both good air stability and high power-conversion efficiency (PCE, of 8.6%). This represents one of the highest PCE values for cyclopenta[2,1-b;3,4-b']dithiophene (CPDT)-based OPVs. This polymer is also utilized for constructing semitransparent solar cells and double-junction tandem solar cells to demonstrate high PCEs of 5.0% and 8.2%, respectively.

1. Introduction

Organic photovoltaics (OPVs) have drawn considerably attention as an economically viable source of renewable energy because of their potential for cost-effective manufacturing, light-weight, and mechanical flexibility.[1–4] So far, bulk hetero-junction (BHJ) OPVs based on conjugated polymers as electron-donor blended with [6,6]-phenyl-C_{71}-butyric acid methyl ester ($PC_{71}BM$) as an electron-acceptor have reached high PCE of over 10%,[5] due to significant progress made in exploiting new materials (e.g. low band-gap (LBG) polymers and fullerene bis-adducts),[3, 6–10] optimization of BHJ morphology through various treatments (e.g., slow growth and processing additive),[8, 11, 12] improvement of interface characteristics through interfacial modifications,[13–15] and development of device architectures (e.g. inverted structure and tandem structure).[8, 13–18] Development of LBG polymers with absorption characteristics that extend into the near-infrared region has drawn intense attention because of the following reasons: (1) They can potential increase the light harvesting ability and thus photocurrent generation of OPVs.[3] (2) They can be combined with a large band-gap polymer in tandem cells to realize complementary absorption.[8, 17, 18] (3) They can be used in a semitransparent OPV that strongly absorbs the light from near-infrared region while allowing most of the visible light to get through.[20, 21]

A straightforward strategy to reduce polymer band-gap is to incorporate both electron-rich and electron-deficient moieties in the conjugated backbone.[3] One of the representative LBG polymers is poly[4,4-bis(2-ethylhexyl)-4H-cyclopenta[2,1-b:3,4-b']dithiophene-2,6-diyl-alt-2,1,3-benzothiadiazole-4,7-diyl] (PCPDTBT),[22] which combines the electron-rich cyclopenta[2,1-b;3,4-b']dithiophene (CPDT) building block with the electron-deficient 2,1,3-benzothiadiazole-4,7-diyl (BT) unit. The BHJ devices based on PCPDTFBT:$PC_{71}BM$ showed a moderate PCE of 5.5%, which is predominately limited by the low V_{oc} value (0.62 V) due to the high-lying

Dr. C.-Y. Chang, L. Zuo, Dr. H.-L. Yip, Y.-X. Li, Dr. C.-Z. Li, Prof. A. K.-Y. Jen, Department of Materials Science and Engineering, University of Washington, Seattle, USA
(E-mail: ajen@u.washington.edu)
Dr. C.-Y. Chang, Prof. C.-S. Hsu, Prof. Y.-J. Cheng, Department of Applied Chemistry, National Chiao Tung University 1001 Ta Hseuh Road, Hsin-Chu 30010, Taiwan
(E-mail: cshsu@mail.nctu.edu.tw)
L. Zuo, Prof. H. Z. Chen, State Key Laboratory of Silicon Materials, MOE Key Laboratory of Macromolecule, Synthesis and Functionalization, Zhejiang-California International Nanosystems Institute, Zhejiang University, Hangzhou 310027, PR China (E-mail: hzchen@zju.edu.cn)
Prof. A. K-Y. Jen (E-mail: ajen@u.washington.edu), Prof. C.-S. Hsu (E-mail: cshsu@mail.nctu.edu.tw), Prof. H. Z. Chen (E-mail: hzchen@zju.edu.cn)

Q2
10.1002/adfm.201301557

ADVANCED FUNCTIONAL MATERIALS

www.afm-journal.de

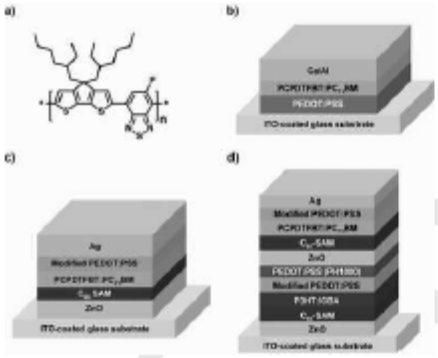

Figure 1. (a) Chemical structure of PCPDTFBT. Schematic representation of the device architecture used in this study: (b) conventional single-junction solar cell, (c) inverted single-junction solar cell and (d) double-junction tandem solar cell.

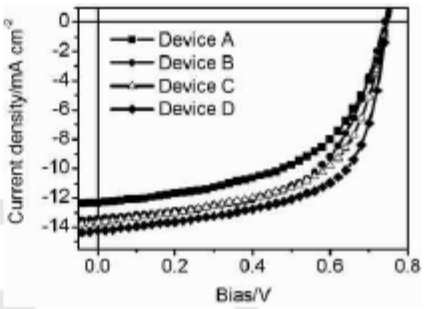

Figure 2. J-V characteristics of the as-fabricated devices (see Table 1 for descriptions of the device types).

highest occupied molecular orbital (HOMO) level of the polymer.[6] The introduction of a strong electron-withdrawing fluoro atom to the electron-deficient unit of polymer has been proven to be effective in lowering the HOMO level of polymer, resulting in increased V_{oc}.[22–26] Moreover, such F-containing polymers can also possess superior hole mobility and preferable morphology as compared with unmodified polymer, leading to the increased J_{sc} and FF.[22–26] Based on this strategy, a F-containing PCPDTBT polymer, poly[2,6-(4,4-bis(2-ethylhexyl)-4H-cyclopenta[2,1-b;3,4-b']dithiophene)-alt-4,7-(5-fluoro-2,1,3-benzothiadiazole)] (PCPDTFBT, chemical structure shown in Figure 1a), has been developed.[24,25]

By adding 1% 1,8-diiodooctane (DIO) as the processing additive to the processing solvent to manipulate the active layer morphology, the PCE of the device has been increased to 6.16%.[25] The DIO is suggested to promote the formation of PCPDFTBT fibrils due to its low vapor pressure (and therefore prolonged evaporation time) and preferential solubility for $PC_{71}BM$, leading to the formation of interpenetrating bicontinuous network within a BHJ film.[25]

In this work, we demonstrate the versatility of PCPDTFBT for OPVs, including the application of it for single-junction solar cells, semitransparent solar cells, and double-junction tandem solar cells. To achieve high performance single-junction cells, 1,3,5-trichlorobenzene (TCB) was used as the solvent to manipulate PCPDTFBT:PC_{71}BM morphology without using any processing additives. The high boiling point TCB prolongs the solvent evaporation time and promotes the crystallization of BHJ film, leading to increased hole mobility and balanced charge transport. By combining the morphological manipulation with interface optimization and device engineering, the single-junction cell exhibits both high PCE (6.6%) and excellent air stability. More importantly, PCPDTFBT can be used to demonstrate highly-efficient semitransparent solar cells (PCE = 5.0%, average visible transmittance (AVT) = 47.3%) and double-junction tandem solar cells (PCE = 8.2%).

2. Results and Discussion

2.1. Conventional Single-Junction Solar Cells

Initially, we investigated the solvent effect on the performance of PCPDTFBT:PC_{71}BM-based single-junction solar cell, with a conventional structure of indium tin oxide (ITO)-coated glass/poly(3,4-ethylenedioxythiophene):poly(styrenesulfonate) (PEDOT:PSS)/active layer/Ca/Al (Figure 1b). Two solvents were examined herein: ortho-dichlorobenzene (ODCB) and TCB. The current–voltage (J-V) characteristics of the devices were shown in Figure 2, and the corresponding device parameters were summarized in Table 1. The ODCB-processed device (Device A) exhibited a short-circuit current density (J_{sc}) of 12.35 mA cm^{-2}, an open-circuit voltage (V_{oc}) of 0.74 V, and a fill factor (FF) of 54.19%, with a PCE of 5.0%, while the TCB-processed device (Device B) showed a relative high PCE of 5.8%, with a J_{sc} of 13.43 mA cm^{-2}, an V_{oc} of 0.74 V, and a FF of 58.05%. Although both ODCB and TCB are good solvents for PCPDTFBT (solubility > 20 mg mL^{-1}), their difference in boiling point (ca. 181 °C for ODCB and ca. 208 °C for TCB) can largely influence the absorption characteristics, crystallinity and morphology of PCPDTFBT:PC_{71} BM BHJ films.

Compared with the UV–vis absorption spectrum of ODCB-cast film, a slight red-shift peak at the long wavelength region (> 650 nm) and a clear vibronic shoulder at 790 nm were observed in the TCB-cast film (Figure S1a), which can be ascribed to stronger interchain interaction and higher ordering of PCPDTFBT. This distinction is more evident in UV-Vis absorption spectra of pure PCPDTFBT films (Figure S1b). To gain more insights into the solvent effect on the microstructure of PCPDTFBT films, X-ray diffraction (XRD) analysis was performed. As shown in Figure 3, ODCB- and TCB-cast films

Table 1. Summary of the photovoltaic device parameters for the single-junction devices.

Device	Conditions[a]	V_{oc} [V]	J_{sc} [mA cm^{-2}]	FF [%]	PCE [%]	μ_h[d] [cm^{2}V^{-1}s^{-1}] : μ_e[d] [cm^{2}V^{-1}s^{-1}]
A	Conventional, ODCB	0.74	12.35	54.19	5.0	3.1×10^{-4} : 2.2×10^{-3}
B	Conventional, TCB	0.74	13.43	58.05	5.8	2.6×10^{-3} : 1.5×10^{-3}
C	Inverted, TCB	0.75	13.70	57.79	6.0	- : -
D	Inverted, TCB[b]	0.74	14.24 (13.95)[c]	61.68	6.6	- : -

[a]Device architecture, solvent; [b]With C_{60}– SAM layer; [c]Calculated from the IPCE spectra shown in Figure 6; [d]Estimated by SCLC model.

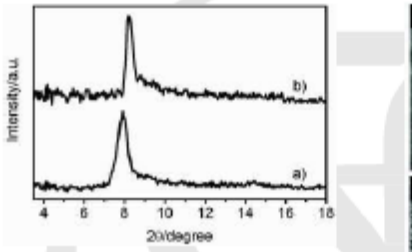

Figure 3. XRD patterns of PCPDTFBT films cast from: (a) ODCB and (b) TCB.

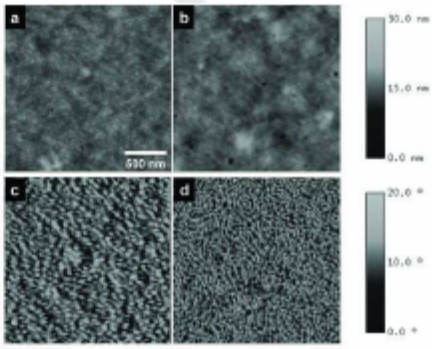

Figure 4. AFM topography (top) and phase (bottom) images of PCPDTFBT:PC_{71}BM films cast from ODCB (a,c) and TCB (b,d). The rms roughness of ODCB- and TCB-cast films is 1.16 nm and 2.28 nm, respectively. The scan size is 2 : m × 2 : m.

8.23° , respectively, corresponding to the (100) reflection of the lamella structure of PCPDTFBT. The solvent-induced change in the diffraction peak position shown in Figure 3 is consistent with previous studies and may result from the self-annealing of crystal defects.[27, 28] The lamellar d-spacing and crystallite size of PCPDTFBT can be obtained from the information of (100) peak using the Bragg's and Scherrer's equation,[29] respectively. As shown in Table 2, compared with ODCB-cast film, TCB-cast film exhibited a slightly smaller lamellar d-spacing (1.07 nm vs. 1.12 nm) and a larger grain size of crystallites (20.69 nm vs. 14.61 nm). These results are in good agreement with the results obtained by UV absorption spectra (Figure S1) and also provide further insights into effective charge transport of TCB- processed film, as discussed below.

The difference in the crystallization between ODCB- and TCB-cast BHJ films was also manifested in the atomic force microscopy (AFM) images (Figure 4): The film cast from TCB exhibited a rougher surface and better defined crystallite fibrils structure than the film cast from ODCB. The root-mean-square (rms) roughnesses are 2.28 and 1.16 nm for TCB- and ODCB-cast films, respectively. To further understand the solvent effect on the charge- transporting properties of the BHJ film, both electron- and hole-only devices were fabricated to estimate charge mobility by the space charge limited current (SCLC) model.

As shown in Table 1 and Figure S2, the TCB-cast film exhibited an increased hole mobility (μ_h) by almost one order of magnitude (from 3.1×10^{-4} cm^{2}V^{-1}s^{-1} to 2.6×10^{-3} cm^{2}V^{-1}s^{-1}) while the electron mobility (μ_e) of the devices remained essentially unchanged (ca. 1.8×10^{-3} cm^2 V^{-1} s^{-1}), leading to the more balance electron/hole mobilities that can effectively reduce space charge build-up within the active layer.[11,30] In view of increased molecular ordering, optimized morphology and enhanced hole mobility, we suggest that high boiling point TCB prolongs the evaporation time to facilitate the self-organization of PCPDTFBT into an optimal morphology, and thus improving device performance.

2.2. Inverted Single-Junction Solar Cells

The inverted structure device have been considered as a potential alternative to achieve higher performance and stability compared to the conventional one due to the removal of susceptible low-work-function metals,[16] preferable vertical phase separation,[31] and favorable distribution of optical field in the inverted device.[32] On the basis of the above reasons, we have evaluated the performance of PCPDTFBT:PC_{71}BM-based single-junction device with the inverted structure (ITO-coated glass/ZnO/active layer/modified PEDOT:PSS/Ag). The inverted device (device C) exhibited a J_{sc} of 13.70 mA cm^{-2}, an V_{oc} of 0.75 V, a FF of 57.79%, and a PCE of 6.0% (Table 1 and

ADVANCED FUNCTIONAL MATERIALS

Table 2. Calculated d-spacing and size of crystallites for PCPDTFBT films cast from ODCB and TCB.

Solvent	d-spacing[a] [nm]	Size of crystallites[b] [nm]
ODCB	1.12	14.61
TCB	1.07	20.69

a)Determined by Bragg's equation; [b]Determined by Scherrer's equation.

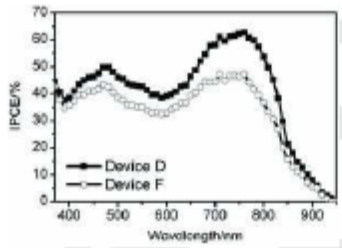

Figure 5. IPCE spectra of the as-fabricated devices (see Table 1 and Table 3 for descriptions of the device types).

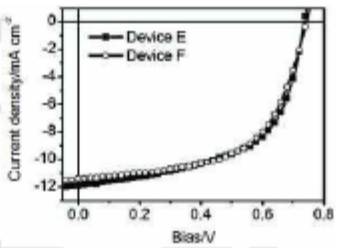

Figure 6. J–V characteristics of the as-fabricated devices (see Table 3 for descriptions of the device types).

Figure 2). By inserting a fullerene self-assembled monolayer (C_{60}-SAM) at the interface between ZnO and the active layer (device D; device structure is shown in Figure 1c), the PCE can be further increased to 6.6%, with a J_{sc} of 14.24 mA cm^{-2}, an V_{oc} of 0.74 V, and a FF of 61.68% (Table 1 and Figure 2). The J_{sc} value of Device D is in good agreement with the values calculated from integrated incident photon-to-current conversion efficiency (IPCE) spectra (Table 1 and Figure 5), which confirms the accuracy of the reported PCE value. It is worth noting that 6.6% represents one of the highest PCE for CPDT-based OPV devices.

The improved PCE obtained from the C_{60}-SAM modified cell is consistent with our previous findings and can be attributed to the passivation of surface traps of ZnO and the enhancement of electronic coupling at the ZnO/active layer interface.[13,14] The effectiveness of the C_{60}-SAM modification is also manifested in increased shunt resistance (i.e. reduced leakage current) and reduced series resistance (i.e. improved charge carrier extraction) of device D compared to those of device C (Table S1 and Figure S3). In addition, the PCE of inverted device D is superior to that of conventional device B (6.6% vs. 5.8%; Table 1), indicating the PCPDTFBT:PC_{71}BM BHJ system is ideal for use in the inverted structure.

More importantly, without encapsulation, device D also possesses good air stability: more than 80% of the initial PCE was retained after more than 2000 h of storage in ambient air (Figure S4; PCE = 5.9%, with a J_{sc} of 12.42 mA cm^{-2}, an V_{oc} of 0.74 V, and a FF of 58.05%). We suggest that this superior air stability may be associated with the low-lying HOMO level of PCPDTFBT afforded by the stronger FBT electron-withdrawing strength.

2.3. Semitransparent Solar Cells

Semitransparent solar cells have great potential to be used in many photovoltaic applications, such as power-generating windows for buildings and automotives.[33–35] Considering the major absorption of PCPDTFBT locates at the near infrared region and most of the visible light is unutilized (Figure 3b), it would be ideal for making semitransparent solar cells. Therefore, we have also applied PCPDTFBT:PC_{71}BM as active BHJ layer in semitransparent solar cell, with a configuration of ITO/ZnO/active layer/PEDOT:PSS/ultra-thin Ag (thickness = 10 or 15 nm). With a 15 nm Ag as the semitransparent top electrode, device E exhibited a reasonable PCE of 5.1% (Table 3 and Figure 6) with a moderate AVT of 39.4% (Figure 7). Interestingly, for device with thinner Ag layer of 10 nm (device F), the AVT can be increased to 47.3% (Figure 7) without compromising its PCE significantly (5.0%; Table 3 and Figure 6), which represents the highest value reported for semitransparent cells with similar transparency. This finding is associated with the good wettability of Ag atoms on the polar PEDOT:PSS layer, which allows Ag atoms to grow homogeneously via Stranski–Krastanov growth model.[36] The effectiveness of PEDOT:PSS seed layer was manifested in more homogeneous morphology with lower rms surface roughness (Figure S5), lower sheet resistance (Table S2), and higher AVT (Figure S6) of 10-nm Ag-coated PEDOT:PSS films compared with those of Ag films deposited without the PEDOT:PSS layer. The photographic image of device F was also shown in inset of Figure 7, where the University of Washington logo can be visualized clearly through the device.

ADVANCED FUNCTIONAL MATERIALS

www.afm-journal.de

Table 4. Summary of the photovoltaic device parameters for the sub-cells and tandem cell.

Device	V_{oc} [V]	J_{sc} [mA cm^{-2}]	FF [%]	PCE [%]
Front cell	0.83	11.59 (10.86)[a]	68.05	6.5
Rear cell	0.74	14.24 (13.95)[b]	61.68	6.6
Tandem cell	1.57	7.83	66.46	8.2

[a]Calculated from the IPCE spectra shown in Figure 6; [b]Calculated from the IPCE spectra shown in Figure S11.

1b. ITO-coated glass substrates (15 Ω cm^{-2}) were cleaned stepwise in detergent, water, acetone, and isopropyl alcohol under ultrasonication for 20 min each and subsequently pretreated by air plasma for 30 min. A PEDOT:PSS layer (Baytron P VP A1 4083) was spin-coated onto the ITO surface. After annealing at 140 ° C for 20 min in air, the substrates were transferred into an N_2-filled glovebox. The active layer (ca. 100 nm) was then spin-cast from the blend solutions of 8 mg mL^{-1} PCPDTFBT

and 20 mg mL^{-1} $PC_{71}BM$ in either ODCB or TCB, followed by annealing at 120 ° C for 10 min. A Ca layer (20 nm) and an Al layer (100 nm) were then deposited under high vacuum (<10^{-6} torr) through a shadow mask, which defined an active area of

0.036 cm^2.

The device architecture of the inverted single-junction solar cell is shown in Figure 1c. A ZnO precursor solution, consisting of 20 mg mL^{-1} zinc acetylacetonate hydrate in anhydrous ethanol, was spin-coated onto cleaned ITO-coated glass, followed by thermal annealing in air at 130 ° C for 5min (ca. 20

nm). Subsequently, a C_{60}-SAM layer was deposited on ZnO using a spin-coating process as previously reported.[14] The substrates were washed with THF twice to remove unbound C_{60}-SAM molecules. The same procedure for the active layer in the conventional device was used for the inverted devices. The modified PEDOT:PSS layer (ca. 70 nm) was then spin-coated from PEDOT:PSS solution (Clevious P VP A1 4083) diluted with equal volume of isopropyl alcohol and 0.2 wt% of Zonyl FSO fluorosurfactant. Afterward, an Ag layer (150 nm) was then deposited under high vacuum (<10^{-6} torr) through a shadow mask, which defined an active area of 0.036 cm^2. Finally, the complete device was thermally annealed at 140 ° C

for 5 min.

Semitransparent Cell Fabrication: The fabrication procedure was the same as that used for the inverted solar cells, except that Ag thickness was controlled to be 10 or 15 nm.

Tandem Cell Fabrication: The device architecture of the tandem solar cell is shown in Figure 1d. ITO-coated glass substrates (15 Ω cm^{-2}) were cleaned stepwise in detergent, water, acetone, and isopropyl alcohol under ultrasonication for 20 min each and subsequently pretreated by air plasma for 30 min. A ZnO precursor solution was then spin-coated onto cleaned ITO-coated glass, followed by thermal annealing in air at 130 ° C for 5 min (ca. 20 nm). Subsequently, a C_{60}-SAM layer was deposited on ZnO. The active layer of the bottom cell was spin-coated from a blend solution of 20 mg mL^{-1} P3HT and

17 mg mL^{-1} ICBA in ODCB, followed by drying the films at room temperature overnight in a closed Petri dish. The modified PEDOT:PSS layer (ca. 80 nm) was then spin-coated from the PEDOT:PSS solution (Clevious P VP A1 4083) diluted with equal volume of isopropyl alcohol and 0.2 wt% of Zonyl FSO fluorosurfactant. After being annealed at 120 ° C for 5 min, PH1000 layer (ca. 40 nm) was spin-coated from its solution (Clevious PH1000) and then annealed at 120 ° C for 5 min. The

surface of the PH1000 layer was then washed with methanol to increase the conductivity and reduce the surface roughness as reported elsewhere.[37] It should be noted that PH1000 layer used herein can ensure the ohmic contact between the modified PEDOT:PSS and ZnO layers. The device without PH1000 layer usually exhibits a S-shaped kink in the J-V characteristics and therefore a deteriorated PCE.

The same procedure for ZnO/C_{60}-SAM layers in the bottom cell was used for the top cell. After that, the active layer (ca. 100 nm) of the top cell was then spin-coated from the blend

solutions of 8 mg mL^{-1} PCPDTFBT and 20 mg mL^{-1} $PC_{71}BM$ in TCB. The modified PEDOT:PSS layer (ca. 70 nm) was then spin-coated from its solution (Clevious P VP A1 4083) diluted with equal volume of isopropyl alcohol and 0.2 wt% of Zonyl FSO fluorosurfactant. Afterward, an Ag layer (250 nm) was then deposited under high vacuum (<10^{-6} torr) through a shadow mask which defined an active area of 0.036 cm^2. Finally, the complete device was thermally annealed at 140 ° C for 5 min.

SCLC Mobility Measurement: The single-carrier mobility can be extracted from the dark J–V characteristics of the hole-only and electron-only devices by using SCLC model:[26,38]

$$J = \frac{9}{8} g_0 g_r : \exp\ 0.891 (\frac{V}{L} \frac{V^2}{L^3}$$

Where g_0 is the permittivity of free space, g_r is the relative permittivity of the material, : is the charge car-

the active area were eliminated using illumination masks with aperture size of 0.0314 cm^2. A Hamamatsu silicon solar cell with a KG5 color filter, which is traced to the National Renewable Energy Laboratory (NREL), was used as the reference cell. To calibrate the light intensity of the solar simulator, the power of the xenon lamp was adjusted to make the J_{SC} of the reference cell under simulated sun light as high as it was under the calibration condition. The spectral mismatches resulting from the test cells, the reference cell, the solar simulator, and the AM1.5 were calibrated with mismatch factors (M). According to Shrotriya et al.,[28d] the mismatch factor is defined as

$$M = \frac{\int_{\lambda 1}^{\lambda 2} E_{Ref}(\lambda) S_R(\lambda) d\lambda \int_{\lambda 1}^{\lambda 2} E_S(\lambda) S_T(\lambda) d\lambda}{\int_{\lambda 1}^{\lambda 2} E_{Ref}(\lambda) S_T(\lambda) d\lambda \int_{\lambda 1}^{\lambda 2} E_S(\lambda) S_R(\lambda) d\lambda}$$

where $E_{Ref}(\lambda)$ is the reference spectral irradiance (AM1.5), $E_S(\lambda)$ is the source spectral irradiance, $S_R(\lambda)$ is the spectral responsivity of the reference cell, and $S_T(\lambda)$ is the spectral responsivity of the test cell, each as a function of wavelength (λ). The spectral responsivities of the test cells and the reference cell were calculated from the corresponding external quantum efficiencies (EQE) by the relationship

$$S(\lambda) = \frac{q\lambda}{hc} EQE(\lambda)$$

where the constant term q/hc equals 8.0655×10^5 for wavelength in units of meters and $S(\lambda)$ in units of AW^{-1}. The Hamamatsu solar cell was also used as the detector for determining the spectral irradiance of the solar simulator. To minimize the spectral transformation, the irradiance spectrum has been calibrated with the spectral responsivity of the Hamamatsu cell and the grating efficiency curve of the monochromator (Oriel Cornerstone 130). UV-Vis absorption spectra were recorded with Perkin-Elmer Lambda-9 spectrophotometer at room temperature. The surface morphology of the polymer films was studied using the tapping mode AFM from a Veeco Nanoscope III controller. The X-ray diffraction spectra of the thin films were recorded using a D8 DISCOVER (Bruker AXS) as the CuK source (wavelength = 1.541 Å) and an output voltage of 40 kV at 40 mA (1600 W). Sheet resistances of the thin films were measured by using a four point probe setup with a source measurement unit (Keithley 2400).

Supporting Information

Supporting Information is available from the Wiley Online Library or from the author.

Acknowledgements

C.-Y. Chang and L. Zuo contributed equally to this work. This work was supported by the AFOSR (FA9550–09–1–0426), the Office of Naval Research (N00014–11–1–0300), and AOARD (FA2386–11–1–4072). A. K.-Y. Jen thanks the Boeing-Johnson Foundation for the financial support.

Received: May 7, 2013
Revised: June 14, 2013
Published Online: MM DD, YYYY

[1] K. M. Coakley, M. D. McGehee, Chem. Mater. 2004, 16, 4533.
[2] B. C. Thompson, J. M. J. Fréchet, Angew. Chem. Int. Ed. 2008, 47, 58.
[3] Y. J. Cheng, S. H. Yang, C. S. Hsu, Chem. Rev. 2009, 109, 5868.
[4] G. Dennler, M. C. Scharber, C. J. Brabec, Adv. Mater. 2009, 21, 1323.
[5] J. You, L. Dou, K. Yoshimura, T. Kato, K. Ohya, T. Moriarty, K. Emery, C.-C. Chen, J. Gao, G. Li, Y. Yang, Nat. Commun. 2013, 4, 1446.
[6] J. Peet, J. Y. Kim, N. E. Coates, W. L. Ma, D. Moses, A. J. Heeger, G. C. Bazan, Nat. Mater. 2007, 6, 497.
[7] G. Zhao, Y. He, Y. Li, Adv. Mater. 2010, 22, 4355.
[8] Y. He, H.-Y. Chen, J. Hou, Y. Li, J. Am. Chem. Soc. 2010, 132, 1377.
[9] Y. Wu, Z. Li, W. Ma, Y. Huang, L. Huo, X. Guo, M. Zhang, H. Ade, J. Hou, Adv. Mater. 2013, DOI: 10.1002/adma.201301174.
[10] Y. Huang, X. Guo, F. Liu, L. Huo, Y. Chen, T. P. Russell, C. C. Han, Y. Li, J. Hou, Adv. Mater. 2012, 24, 3383.
[11] G. Li, V. Shrotriya, J. Huang, Y. Yao, T. Moriarty, K. Emery, Y. Yang, Nat. Mater. 2005, 4, 864.
[12] J. K. Lee, W. L. Ma, C. J. Brabec, J. Yuen, J. S. Moon, J. Y. Kim, K. Lee, G. C. Bazan, A. J. Heeger, J. Am. Chem. Soc. 2008, 130, 3619.
[13] S. K. Hau, H.-L. Yip, O. Acton, N. S. Baek, H. Ma, A. K. Y. Jen, J. Mater. Chem. 2008, 18, 5113.
[14] S. K. Hau, H.-L. Yip, H. Ma, A. K. Y. Jen, Appl. Phys. Lett. 2008, 93, 233304.
[15] T. Yang, M. Wang, C. Duan, X. Hu, L. Huang, J. Peng, F. Huang, X. Gong, Energy Environ. Sci. 2012, 5, 8208.
[16] S. K. Hau, H.-L. Yip, N. S. Baek, J. Zou, K. O'Malley, A. K. Y. Jen, Appl. Phys. Lett. 2008, 92, 253301.
[17] L. Dou, J. You, J. Yang, C.-C. Chen, Y. He, S. Murase, T. Moriarty, K. Emery, G. Li, Y. Yang, Nat. Photon. 2012, 6, 180.
[18] J. Y. Kim, K. Lee, N. E. Coates, D. Moses, T.-Q. Nguyen, M. Dante, A. J. Heeger, Science 2007, 317, 222.
[19] S. K. Hau, H.-L. Yip, K.-S. Chen, J. Zou, A. K.-Y. Jen, Appl. Phys. Lett. 2010, 97, 253307.
[20] L. Dou, W.-H. Chang, J. Gao, C.-C. Chen, J. You, Y. Yang, Adv. Mater. 2013, 25, 825.
[21] C.-C. Chen, L. Dou, R. Zhu, C.-H. Chung, T.-B. Song, Y. B. Zheng, S. Hawks, G. Li, P. S. Weiss, Y. Yang, ACS Nano 2012, 6, 7185.
[22] H. Zhou, L. Yang, A. C. Stuart, S. C. Price, S. Liu, W. You, Angew. Chem. Int. Ed. 2011, 50, 2995.
[23] A. C. Stuart, J. R. Tumbleston, H. Zhou, W. Li, S. Liu, H. Ade, W. You, J. Am. Chem. Soc. 2013, 135, 1806.
[24] Y. Zhang, J. Zou, C.-C. Cheun, H.-L. Yip, A. K. Y. Jen, Macromolecules 2012, 45, 5427.
[25] S. Albrecht, S. Janietz, W. Schindler, J. Frisch, J. Kurpiers, J. Kniepert, S. Inal, P. Pingel, K. Fostiropoulos, N. Koch, D. Neher, J. Am. Chem. Soc. 2012, 134, 14932.
[26] H. Bronstein, J. M. Frost, A. Hadipour, Y. Kim, C. B. Nielsen, R. S. Ashraf, B. P. Rand, S. Watkins, I. McCulloch, Chem. Mater. 2013, 25, 277.
[27] T. Wang, A. D. F. Dunbar, P. A. Staniec, A. J. Pearson, P. E. Hopkinson, J. E. MacDonald, S. Lilliu, C. Pizzey, N. J. Terrill, A. M. Donald, A. J. Ryan, R. A. L. Jones, D. G. Lidzey, Soft Matter 2010, 6, 4128.

ADVANCED FUNCTIONAL MATERIALS

www.afm-journal.de

[28] C.-W. Chu, H. Yang, W.-J. Hou, J. Huang, G. Li, Y. Yang, Appl. Phys. Lett. 2008, 92, 103306.
[29] B. D. Cullity, Elements of X-ray Diffraction, Addison-Wesley Pub. Co., Reading, Mass, USA 1956.
[30] V. D. Mihailetchi, H. Xie, B. De Boer, L. J. A. Koster, P. W. M. Blom, Adv. Funct. Mater. 2006, 16, 699.
[31] Z. Xu, L.-M. Chen, G. Yang, C.-H. Huang, J. Hou, Y. Wu, G. Li, C.-S. Hsu, Y. Yang, Adv. Funct. Mater. 2009, 19, 1227.
[32] S. Albrecht, S. Schäfer, I. Lange, S. Yilmaz, I. Dumsch, S. Allard, U. Scherf, A. Hertwig, D. Neher, Org. Electron. 2012, 13, 615.
[33] K.-S. Chen, J.-F. Salinas, H.-L. Yip, L. Huo, J. Hou, A. K. Y. Jen, Energy Environ. Sci. 2012, 5, 9551.
[34] C.-C. Chueh, S.-C. Chien, H.-L. Yip, J. F. Salinas, C.-Z. Li, K.-S. Chen, F.-C. Chen, W.-C. Chen, A. K. Y. Jen, Adv. Energy Mater. 2013, 3, 417.
[35] Z. Tang, Z. George, Z. Ma, J. Bergqvist, K. Tvingstedt, K. Vandewal, E. Wang, L. M. Andersson, M. R. Andersson, F. Zhang, O. Inganäs, Adv. Energy Mater. 2012, 2, 1467.
[36] L. Ke, S.C. Lai, H. Liu, C.K.N. Peh, B. Wang, J. H. Teng, ACS Appl. Mater. Inter. 2012, 4, 1247.
[37] D. Alemu, H.-Y. Wei, K.-C. Ho, C.-W. Chu, Energy Environ.Sci. 2012, 5, 9662.
[38] M. F. Falzon, M. M. Wienk, R. A. J. Janssen, J. Phys. Chem. C 2011, 115, 3178.
[39] V. Shrotriya, G. Li, Y. Yao, T. Moriarty, K. Emery, Y. Yang, Adv.

Polymer Chemistry

RSC Publishing

COMMUNICATION

View Article Online
View Journal

Indacenodithieno[3,2-*b*]thiophene-based broad bandgap polymers for high efficiency polymer solar cells†

Cite this: DOI: 10.1039/c3py00121k

Received 23rd January 2013
Accepted 7th March 2013

DOI: 10.1039/c3py00121k

www.rsc.org/polymers

Yun-Xiang Xu,[a] Chu-Chen Chueh,[a] Hin-Lap Yip,[a] Chih-Yu Chang,[a] Po-Wei Liang,[a] Jeremy J. Intemann,[a] Wen-Chang Chen[b] and Alex K.-Y. Jen*[a]

Two broad bandgap polymers, poly{(indacenodithieno[3,2-*b*]thiophene)-*alt*-[2,5-bis(thiophen-2-yl)thiazolo[5,4-*d*]thiazole-5,5′-diyl]} PIDTT-TzTz and poly{(indacenodithieno[3,2-*b*]thiophene)-*alt*-[2,5-bis(6-octylthieno[3,2-*b*]thiophen-2-yl)thiazolo[5,4-*d*]thiazole-5,5′-diyl]} PIDTT-TzTz-TT, were designed and synthesized by copolymerizing the ladder-type indacenodithieno[3,2-*b*]thiophene (IDTT) donor with a thiazolothiazole (TzTz) acceptor. Both polymers possess moderate hole-mobilities of around $\sim 10^{-4}$ cm^2 V^{-1} s^{-1}. The polymer solar cells (PSCs) using PIDTT-TzTz–$PC_{71}BM$ as the active layer showed good power conversion efficiencies (PCEs as high as 5.53% and 5.90%) in both conventional and inverted devices, without using any solvent additives. These results demonstrate that these broad bandgap PIDTT-TzTz polymers have potential to be used as a front cell for polymer tandem cells.

Tremendous progress has been made in recent years on the development of organic photovoltaic materials, especially donor–acceptor (D–A) polymers, which have achieved an impressive photovoltaic performance of over 9% efficiency, when blended with fullerene derivatives.[1,2] Among semiconducting polymers, broad bandgap (BBG) materials have attracted a lot of attention because of their potential applications in tandem solar cells[3–5] and semi-transparent materials.[6–9] To date, regioregular poly(3-hexylthiophene) (P3HT) is one of the most representative BBG polymers. High photovoltaic performances of P3HT have been accomplished by utilizing indene–C_{60} (or C_{70}) bis-adducts as the electron acceptor in bulk heterojunction (BHJ) devices.[10–12] However, the long-term oxidative stability of P3HT is an issue due to its high-lying HOMO level, as well as film uniformity and reproducibility when it is used in large scale roll-to-roll printing because of P3HT's sensitivity to the processing conditions. To solve these issues, other alternative materials have been developed. The approach of using a D–A polymer is an attractive way to develop conjugated polymers due to easy tuning of their bandgaps and energy levels. From a molecular design viewpoint, weak donors are usually adopted in the polymer structure to ensure a low-lying HOMO level, which is closely correlated with the open-circuit voltage (V_{oc}) of polymer photovoltaic devices.[13] Many different kinds of donor structures have been utilized in BBG polymers, such as fluorene, carbazole, benzodithiophene (BDT), and indacenodithiophene (IDT).[14–19] Meanwhile, the incorporated acceptor moieties have included 4,7-di(thiophen-2-yl)-2,1,3-benzothiadiazole (DTBT), 4,4′-dihexyl-2,2′-bithiazole (BTz), or 2,5-bis(thiophen-2-yl)thiazolo[5,4-*d*]thiazole (TzTz).[20,21] High power conversion efficiencies (PCEs) have been obtained through subtle choices of donor and acceptor segments and tuning the side-chain structures.[20,22] For example, PCDTBT, with a bandgap of 1.88 eV, prepared by copolymerizing 2,7-carbazole and DTBT, showed a high PCE above 6%.[14,15] Janssen and co-workers further incorporated this BBG polymer into tandem solar cells, which resulted in a higher PCE of greater than 7% for their best devices.[3] Nevertheless, compared to well-developed low bandgap polymers, BBG polymers remain less explored, especially while considering other aspects in addition to photovoltaic performance, such as long-term stability and ease of processing. It is highly desirable to design and synthesize new BBG materials to fulfil these requirements.

Ladder-type donors have been widely utilized in D–A polymers.[23–29] These large fused-ring moieties usually result in polymers with high charge carrier mobilities due to reduced reorganizational energies and good solubility in common organic solvents. Amorphous materials are usually obtained based on ladder-type donors possessing cyclopentadiene rings because the out-of-plane side-chains prevent ordered packing of polymer backbones. Therefore, the morphologies of the as-prepared films of polymers or fullerene blends are not sensitive to processing conditions according to our previous studies,[30,31] an important requirement for the commercialization of

[a]Department of Materials Science and Engineering, University of Washington, Seattle, WA 98195, USA. E-mail: ajen@u.washington.edu

[b]Department of Chemical Engineering, Institute of Polymer Science and Engineering, National Taiwan University, Taipei 106, Taiwan

† Electronic supplementary information (ESI) available: See DOI: 10.1039/c3py00121k

polymer solar cells. Moreover, impressive stability can be achieved based on ladder-type systems according to Cheng's work.[32] The stable morphology of polymer films contributed greatly to the overall stability of the device.

Indacenodithieno[3,2-*b*]thiophene (IDTT) is a relatively new ladder-type donor, which features improved mobility and absorption coefficients of its polymers when compared to IDT-based polymers.[31] We believed that this donor would be an ideal segment for BBG polymers because it will not only enhance the mobility of the resulting polymers but also its weak donating strength should result in a deep-lying HOMO level, which is good for oxidative stability and critical to obtain a high V_{oc} in photovoltaic devices.

In this communication, two copolymers based on the IDTT donor were synthesized and investigated, namely PIDTT-TzTz and PIDTT-TzTz-TT (Scheme 1). TzTz was chosen as the acceptor moiety because of its rigid coplanar structure, which will not only facilitate π-electron delocalization but also enhance π–π stacking of the polymer backbone. TzTz-based polymers have also exhibited high mobilities in field-effect transistors (FET)[33] and good photovoltaic performances.[16,19] In these two polymers, thiophene and thieno[3,2-*b*]thiophene (TT) were used as π-bridges, which was expected to increase the effective conjugation length and enhance intermolecular charge hopping between polymers.[34,35] However, PIDTT-TzTz-TT-based devices only showed a moderate PCE (4.4%), probably due to their poor solubility leading to un-optimized phase separation with $PC_{71}BM$. Encouragingly, PIDTT-TzTz derived devices showed high PCEs of 5.53% and 5.90%, respectively in regular and inverted solar cell architectures, which makes it one of the best performing BBG polymers for PSCs.

PIDTT-TzTz and PIDTT-TzTz-TT were synthesized *via* the Stille cross-coupling polymerization reaction with palladium catalyst, the details of which can be found in the ESI.† PIDTT-TzTz has moderate solubility in hot chlorobenzene (CB) and dichlorobenzene (DCB) while PIDTT-TzTz-TT is only soluble in hot DCB. The number-average molecular weights of PIDTT-TzTz and PIDTT-TzTz-TT were 26 kDa and 34 kDa, respectively, with polydispersity indices (PDI) of 4.18 and 3.91. Differential scanning calorimetry of the polymers showed no apparent thermal transitions for either of the polymers between 20 °C and 280 °C.

The UV-vis absorption spectra of the two polymers in DCB solutions and in films are shown in Fig. 1. For PIDTT-TzTz, an absorption peak at 569 nm was observed in the DCB solution

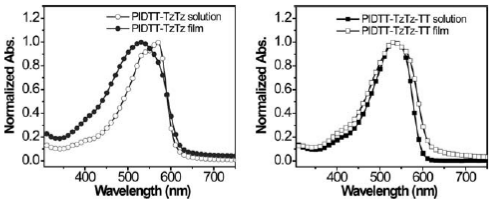

Fig. 1 UV-vis spectra of (a) PIDTT-TzTz and (b) PIDTT-TzTz-TT in dichlorobenzene solution and film state.

while its maximum peak in the film was blue-shifted to 531 nm, probably due to twisting of the polymer backbone when the polymer chains were forced to pack together. Notably, PIDTT-TzTz-TT showed the same absorption maxima in both solution and film states, which can be ascribed to the increased rigidity and coplanarity of its backbone compared to PIDTT-TzTz.[36] Both polymers possess a broad optical bandgap (E_g) of 2.0 eV according to the onsets of film spectra at around 620 nm.

The energy levels of both polymers were estimated by cyclic voltammetry measurements. The corresponding redox curves are shown in Fig. S1 of the ESI.† The corresponding HOMO and LUMO energy levels for PIDTT-TzTz and PIDTT-TzTz-TT are (−5.24, −3.21) and (−5.34, −3.03) eV, respectively. Owing to the incorporated IDTT donor moiety, both polymers possess reasonably low-lying HOMO levels, which is promising for achieving high V_{oc} in their photovoltaic devices.[31] The even lower-lying HOMO level of PIDTT-TzTz-TT compared to that of PIDTT-TzTz is probably due to the higher aromaticity of the TT π-bridge unit relative to the thiophene unit.[37,38] The high-lying LUMO levels of both polymers guarantee sufficient energy offsets to drive charge separation at the interface between the polymer and $PC_{71}BM$ in photovoltaic devices.

Charge mobilities of pristine polymers in FET devices were investigated with a bottom gate/top contact configuration. The corresponding transfer curves are shown in Fig. S2 of the ESI† and relevant parameters are summarized in Table 1. PIDTT-TzTz-TT showed a saturated hole mobility of 7.0×10^{-4} cm^2 V^{-1} s^{-1}, slightly higher than that of PIDTT-TzTz (1.5×10^{-4} cm^2 V^{-1} s^{-1}). This result suggests that the extended TT bridge in PIDTT-TzTz-TT indeed improves hole transportation, due to the increased coplanarity of the polymer backbone and enhanced intermolecular charge hopping compared to PIDTT-TzTz.[34]

Photovoltaic properties of both polymers were investigated initially with a BHJ device configuration of ITO/PEDOT:PSS/polymer:$PC_{71}BM$/bis-C_{60}/Ag under the illumination of AM 1.5G at 100 mA cm^{-2} (Fig. S3 of the ESI†).[39–42] Typical *J*–*V* curves of the devices are shown in Fig. 2a and the performance of these devices is summarized in Table 2. The PIDTT-TzTz device

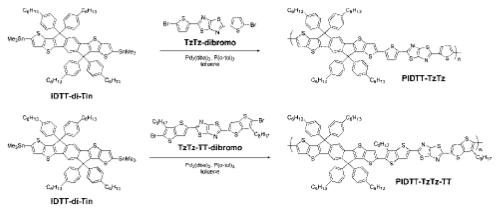

Scheme 1 Chemical structures and synthetic routes of PIDTT-TzTz and PIDTT-TzTz-TT.

Table 1 FET characteristics of PIDTT-TzTz and PIDTT-TzTz-TT

Polymer	Hole mobility (cm^2 V^{-1} s^{-1})	On/off ratio	V_t (V)
PIDTT-TzTz	1.5×10^{-4}	6.6×10^3	−29.6
PIDTT-TzTz-TT	7×10^{-4}	2.5×10^4	−19.8

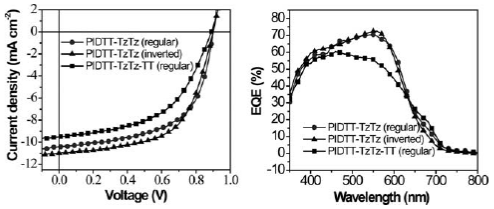

Fig. 2 (a) Characteristic *J–V* curves for the BHJ solar cells derived from PIDTT-TzTz (circles for a regular device and triangles for an inverted device) and PIDTT-TzTz-TT (squares for a regular device) under 1 Sun condition (100 mW cm^{-2}). (b) EQE spectra for the BHJ devices derived from PIDTT-TzTz and PIDTT-TzTz-TT.

Table 2 Photovoltaic properties of PSCs based on the polymers as donors and $PC_{71}BM$ as the acceptor under the illumination of AM 1.5G, 100 mW cm^{-2}

BHJ layer	V_{oc} (V)	J_{sc} (mA cm^{-2})	FF	PCE (%)
PIDTT-TzTz–$PC_{71}BM$ (regular device)	0.90	10.41	0.59	5.53
PIDTT-TzTz–$PC_{71}BM$ (inverted device)	0.90	10.99	0.59	5.90
PIDTT-TzTz-TT–$PC_{71}BM$ (regular device)	0.89	9.51	0.52	4.40

showed an impressive PCE of 5.53% with a V_{oc} of 0.90 V, a J_{sc} of 10.41 mA cm^{-2}, and a FF of 0.59 without the use of any processing additives or post-treatment, while the device made from PIDTT-TzTz-TT gave a similar V_{oc} of 0.89 V, an inferior J_{sc} of 9.51 mA cm^{-2} and a FF of 0.52, resulting in a lower PCE of 4.4%. Although PIDTT-TzTz-TT has a higher hole mobility than PIDTT-TzTz, the lower J_{sc} and FF of PIDTT-TzTz-TT-based devices can be attributed to their inferior solubility, which reduces the polymer composition in the BHJ layer and leads to an un-optimized morphology. Atomic force microscopy (AFM) images were acquired to investigate the difference of morphologies of BHJ layers (Fig. S4†). A relatively smoother thin film morphology was observed for the PIDTT-TzTz-based BHJ layer, coinciding with the better phase separation in this active layer, resulting in higher performance of devices.

Since inverted polymer solar cells have the advantages of high air stability, preferred vertical composition gradient and compatibility with roll-to-roll printing techniques, they have been widely explored using various materials, including BBG polymers.[43–45] Therefore, PIDTT-TzTz was further explored using an inverted architecture (Fig. S5 of the ESI†). As shown in Fig. 2a and Table 2, the inverted configuration led to a superior device performance compared to the conventional device architecture, possessing a V_{oc} of 0.90 V, a J_{sc} of 10.99 mA cm^{-2}, and a FF of 0.59, giving a PCE of 5.90%.

The external quantum efficiencies (EQEs) of polymer–$PC_{71}BM$ devices with both regular and inverted architectures were measured and are shown in Fig. 2b. All the J_{sc} values calculated from the EQE curves under the standard AM 1.5G conditions match well with those obtained from the *J–V* measurements. Notably, the PIDTT-TzTz device has a high EQE of 70% around 550 nm, which ensures the efficient light-absorbing ability of this BBG polymer.

In conclusion, two BBG polymers PIDTT-TzTz and PIDTT-TzTz-TT have been designed and synthesized based on the ladder-type donor, IDTT. Both polymers possess moderate hole-mobilities of around $\sim 10^{-4}$ cm^2 V^{-1} s^{-1}. High photovoltaic performance with PCEs of 5.53% and 5.90% could be obtained for PIDTT-TzTz in conventional and inverted device architectures, respectively, without the use of any solvent additives. These are among the highest performances reported for BBG polymers. When these promising results are combined with a large bandgap (E_g = 2.0 eV), easy processing, and a low-lying HOMO level, it makes PIDTT-TzTz an ideal material for incorporating into the front part of the tandem solar cells or semi-transparent solar cells for energy producing windows.

Notes and references

1 Z. He, C. Zhong, S. Su, M. Xu, H. Wu and Y. Cao, *Nat. Photonics*, 2012, **6**, 593–597.
2 L. Dou, W.-H. Chang, J. Gao, C.-C. Chen, J. You and Y. Yang, *Adv. Mater.*, 2013, **25**, 825–831.
3 V. S. Gevaerts, A. Furlan, M. M. Wienk, M. Turbiez and R. A. J. Janssen, *Adv. Mater.*, 2012, **24**, 2130–2134.
4 S. Kouijzer, S. Esiner, C. H. Frijters, M. Turbiez, M. M. Wienk and R. A. J. Janssen, *Adv. Energy Mater.*, 2012, **2**, 945–949.
5 L. Dou, J. You, J. Yang, C.-C. Chen, Y. He, S. Murase, T. Moriarty, K. Emery, G. Li and Y. Yang, *Nat. Photonics*, 2012, **6**, 180–185.
6 J. Huang, G. Li and Y. Yang, *Adv. Mater.*, 2008, **20**, 415–419.
7 Y. Zhou, H. Cheun, S. Choi, W. J. Potscavage, Jr, C. Fuentes-Hernandez and B. Kippelen, *Appl. Phys. Lett.*, 2010, **97**, 153304.
8 Y.-Y. Lee, K.-H. Tu, C.-C. Yu, S.-S. Li, J.-Y. Hwang, C.-C. Lin, K.-H. Chen, L.-C. Chen, H.-L. Chen and C.-W. Chen, *ACS Nano*, 2011, **5**, 6564–6570.
9 J. Czolk, A. Puetz, D. Kutsarov, M. Reinhard, U. Lemmer and A. Colsmann, *Adv. Energy Mater.*, 2013, **3**, 386–390.
10 G. Zhao, Y. He and Y. Li, *Adv. Mater.*, 2010, **22**, 4355–4358.
11 Y.-J. Cheng, C.-H. Hsieh, Y. He, C.-S. Hsu and Y. Li, *J. Am. Chem. Soc.*, 2010, **132**, 17381–17383.
12 X. Guo, C. Cui, M. Zhang, L. Huo, Y. Huang, J. Hou and Y. Li, *Energy Environ. Sci.*, 2012, **5**, 7943–7949.
13 M. C. Scharber, D. Wuhlbacher, M. Koppe, P. Denk, C. Waldauf, A. J. Heeger and C. L. Brabec, *Adv. Mater.*, 2006, **18**, 789–794.
14 N. Blouin, A. Michaud and M. Leclerc, *Adv. Mater.*, 2007, **19**, 2295–2300.
15 S. H. Park, A. Roy, S. Beaupre, S. Cho, N. Coates, J. S. Moon, D. Moses, M. Leclerc, K. Lee and A. J. Heeger, *Nat. Photonics*, 2009, **3**, 297–302.
16 L. Huo, X. Guo, S. Zhang, Y. Li and J. Hou, *Macromolecules*, 2011, **44**, 4035–4037.
17 Q. Shi, H. Fan, Y. Liu, W. Hu, Y. Li and X. Zhan, *Macromolecules*, 2011, **44**, 9173–9179.
18 S. C. Price, A. C. Stuart, L. Yang, H. Zhou and W. You, *J. Am. Chem. Soc.*, 2011, **133**, 4625–4631.

19 M. Zhang, X. Guo, X. Wang, H. Wang and Y. Li, *Chem. Mater.*, 2011, **23**, 4264–4270.
20 R. Qin, W. Li, C. Li, C. Du, C. Veit, H.-F. Schleiermacher, M. Andersson, Z. Bo, Z. Liu, O. Inganas, U. Wuerfel and F. Zhang, *J. Am. Chem. Soc.*, 2009, **131**, 14612–14613.
21 X. Zhao, D. Yang, H. Lv, L. Yin and X. Yang, *Polym. Chem.*, 2013, **4**, 57–60.
22 S. K. Lee, J. M. Cho, Y. Goo, W. S. Shin, J.-C. Lee, W.-H. Lee, I.-N. Kang, H.-K. Shim and S.-J. Moon, *Chem. Commun.*, 2011, **47**, 1791–1793.
23 C. P. Chen, S. H. Chan, T. C. Chao, C. Ting and B. T. Ko, *J. Am. Chem. Soc.*, 2008, **130**, 12828–12833.
24 Q. Zheng, B. J. Jung, J. Sun and H. E. Katz, *J. Am. Chem. Soc.*, 2010, **132**, 5394–5404.
25 H.-H. Chang, C.-E. Tsai, Y.-Y. Lai, D.-Y. Chiou, S.-L. Hsu, C.-S. Hsu and Y.-J. Cheng, *Macromolecules*, 2012, **45**, 9282–9291.
26 I. McCulloch, R. S. Ashraf, L. Biniek, H. Bronstein, C. Combe, J. E. Donaghey, D. I. James, C. B. Nielsen, B. C. Schroeder and W. Zhang, *Acc. Chem. Res.*, 2012, **45**, 714–722.
27 X. Guo, M. Zhang, J. Tan, S. Zhang, L. Huo, W. Hu, Y. Li and J. Hou, *Adv. Mater.*, 2012, **24**, 6536–6541.
28 Y. Zhang, S.-C. Chien, K.-S. Chen, H.-L. Yip, Y. Sun, J. A. Davies, F.-C. Chen and A. K. Y. Jen, *Chem. Commun.*, 2011, **47**, 11026–11028.
29 Y. Zhang, J. Zou, H.-L. Yip, K.-S. Chen, D. F. Zeigler, Y. Sun and A. K. Y. Jen, *Chem. Mater.*, 2011, **23**, 2289–2291.
30 Y. Zhang, J. Zou, H.-L. Yip, K.-S. Chen, J. A. Davies, Y. Sun and A. K. Y. Jen, *Macromolecules*, 2011, **44**, 4752–4758.
31 Y.-X. Xu, C.-C. Chueh, H.-L. Yip, F.-Z. Ding, Y.-X. Li, C.-Z. Li, X. Li, W.-C. Chen and A. K. Y. Jen, *Adv. Mater.*, 2012, **24**, 6356–6361.
32 C.-Y. Chang, Y.-J. Cheng, S.-H. Hung, J.-S. Wu, W.-S. Kao, C.-H. Lee and C.-S. Hsu, *Adv. Mater.*, 2012, **24**, 549–553.
33 I. Osaka, R. Zhang, G. Sauvé, D.-M. Smilgies, T. Kowalewski and R. D. McCullough, *J. Am. Chem. Soc.*, 2009, **131**, 2521–2529.
34 H. Bronstein, Z. Chen, R. S. Ashraf, W. Zhang, J. Du, J. R. Durrant, P. Shakya Tuladhar, K. Song, S. E. Watkins, Y. Geerts, M. M. Wienk, R. A. J. Janssen, T. Anthopoulos, H. Sirringhaus, M. Heeney and I. McCulloch, *J. Am. Chem. Soc.*, 2011, **133**, 3272–3275.
35 X. Wang, Y. Sun, S. Chen, X. Guo, M. Zhang, X. Li, Y. Li and H. Wang, *Macromolecules*, 2012, **45**, 1208–1216.
36 S. Ko, E. T. Hoke, L. Pandey, S. Hong, R. Mondal, C. Risko, Y. Yi, R. Noriega, M. D. McGehee, J.-L. Brédas, A. Salleo and Z. Bao, *J. Am. Chem. Soc.*, 2012, **134**, 5222–5232.
37 G. Subramanian, P. von Ragué Schleyer and H. Jiao, *Angew. Chem., Int. Ed.*, 1996, **35**, 2638–2641.
38 Y.-J. Cheng, S.-W. Cheng, C.-Y. Chang, W.-S. Kao, M.-H. Liao and C.-S. Hsu, *Chem. Commun.*, 2012, **48**, 3203–3205.
39 G. Yu, J. Gao, J. C. Hummelen, F. Wudl and A. J. Heeger, *Science*, 1995, **270**, 1789.
40 K. M. O'Malley, C.-Z. Li, H.-L. Yip and A. K. Y. Jen, *Adv. Energy Mater.*, 2012, **2**, 82–86.
41 C.-Z. Li, C.-C. Chueh, H.-L. Yip, K. M. O'Malley, W.-C. Chen and A. K. Y. Jen, *J. Mater. Chem.*, 2012, **22**, 8574–8578.
42 C.-Z. Li, H.-L. Yip and A. K. Y. Jen, *J. Mater. Chem.*, 2012, **22**, 4161–4177.
43 Y. Sun, J. H. Seo, C. J. Takacs, J. Seifter and A. J. Heeger, *Adv. Mater.*, 2011, **23**, 1679–1683.
44 J. Sun, Y. Zhu, X. Xu, L. Lan, L. Zhang, P. Cai, J. Chen, J. Peng and Y. Cao, *J. Phys. Chem. C*, 2012, **116**, 14188–14198.
45 S. K. Hau, H.-L. Yip and A. K. Y. Jen, *Polym. Rev.*, 2010, **50**, 474–510.